Inorganic Chemistry

pubs.acs.org/IC

Article

Evaluation of the Effect of Macrocyclic Ring Size on [^{203}Pb]Pb(II) Complex Stability in Pyridyl-Containing Chelators

Brooke L. McNeil, Karthika J. Kadassery, Anthony W. McDonagh, Wen Zhou, Paul Schaffer, Justin J. Wilson, and Caterina F. Ramogida*

Cite This: *Inorg. Chem.* 2022, 61, 9638–9649

Read Online

ACCESS | Metrics & More | Article Recommendations | Supporting Information

ABSTRACT: As an element-equivalent theranostic pair, lead-203 (^{203}Pb, 100% EC, half-life = 51.92 h) and lead-212 (^{212}Pb, 100% β^-, half-life = 10.64 h), through the emission of γ rays and an α particle in its decay chain, respectively, can aid in the development of personalized targeted radionuclide treatment for advanced and currently untreatable cancers. With these isotopes currently being used in clinical trials, an understanding of the relationship between the chelator structure, ability to incorporate the radiometal, and metal−complex stability is needed to help design appropriate chelators for clinical use. Herein, we report an investigation into the effect of ring size in macrocyclic chelators where pyridine, an intermediate Lewis base, acts as an electron donor toward lead. Crown-4Py (4,7,13,16-tetrakis(pyridin-2-ylmethyl)-1,10-dioxa-4,7,13,16-tetraazacyclooctadecane), cyclen-4Py (1,4,7,10-tetrakis(pyridin-2-ylmethyl)-1,4,7,10-tetraazacyclododecane), and NOON-2Py (7,16-bis(pyridin-2-ylmethyl)-1,4,10,13-tetraoxa-7,16-diazacyclooctadecane) were synthesized and analyzed for their ability to coordinate Pb^{2+}. Metal complex stability was investigated via [^{203}Pb]Pb^{2+} radiolabeling studies, ^{1}H NMR spectroscopy, X-ray crystallography, and potentiometry. With the smallest macrocyclic backbone, cyclen-4Py had the highest radiochemical yield, while, in descending order, crown-4Py and NOON-2Py had the lowest. Thermodynamic stability constants (log K_{ML}) of 19.95(3), 13.29(5), and 11.67 for $[Pb(Cyclen\text{-}4Py)]^{2+}$, $[Pb(Crown\text{-}4Py)]^{2+}$, and $[Pb(NOON\text{-}2Py)]^{2+}$, respectively, correlated with their radiochemical yields. The X-ray crystal structure of the least stable complexes $[Pb(NOON\text{-}2Py)]^{2+}$ revealed a hemidirected Pb^{2+} center, as reflected by a void within the coordination sphere, and $[Pb(Crown\text{-}4Py)]^{2+}$ showed an average Pb−N pyridine interatomic distance of >3 Å. By contrast, the crystal structure of $[Pb(Cyclen\text{-}4Py)]^{2+}$ showed shorter Pb−N pyridine interactions, and in solution, only one highly symmetric isomer existed for this complex, whereas conformational flexibility was observed for both $[Pb(Crown\text{-}4Py)]^{2+}$ and $[Pb(NOON\text{-}2Py)]^{2+}$ at the NMR timescale. This study illustrates the importance of the macrocyclic backbone size when incorporating bulky electron-donor groups into the design of a macrocyclic chelator as it affects the accessibility of lead to the donor arms. Our results show that cyclen-4Py is a promising chelator for future studies with this theranostic pair.

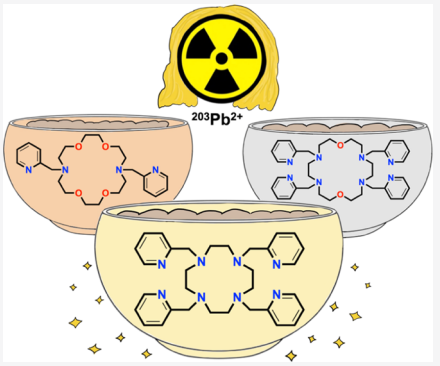

Downloaded via CORNELL UNIV on July 20, 2022 at 13:39:01 (UTC).
See https://pubs.acs.org/sharingguidelines for options on how to legitimately share published articles.

INTRODUCTION

The bifunctional chelator (BFC) approach is a common strategy employed in the development of novel radiopharmaceuticals.[1] More specifically, the BFC approach in the field of radiopharmaceutical development involves tissue-specific delivery of a radioactive payload through the use of a chelator coordinating a radioactive metal (radiometal), which is attached via a linker to a biological targeting vector. This vector−chelate−isotope complex is then injected to selectively seek out and bind its cancer biomarker. In the context of radionuclide therapy, this highly selective and direct delivery of radiation allows for reduced side effects on healthy cells compared to existing methods.[2] This technique is also intriguing as it enables a personalized approach to healthcare by pairing both photon- and particle-emitting isotopes, which in turn allows clinicians to assess radiopharmaceutical uptake via imaging prior to therapy. This pairing of both a *thera*peutic and diag*nostic* form of a radiopharmaceutical is referred to as *theranostics*. Radiometals that emit cytotoxic alpha(α) particles, beta(β^-) particles, or Meitner−Auger electrons (MAEs) are compatible with therapy, while those that emit photons, through decay processes such as electron capture (EC) or positron emission (β^+ decay), are compatible with imaging techniques such as single-photon emission computed tomography (SPECT) and positron emission tomography (PET), respectively.

Received: April 2, 2022
Published: June 15, 2022

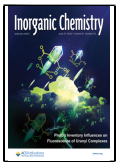

© 2022 American Chemical Society

https://doi.org/10.1021/acs.inorgchem.2c01114
Inorg. Chem. 2022, 61, 9638−9649

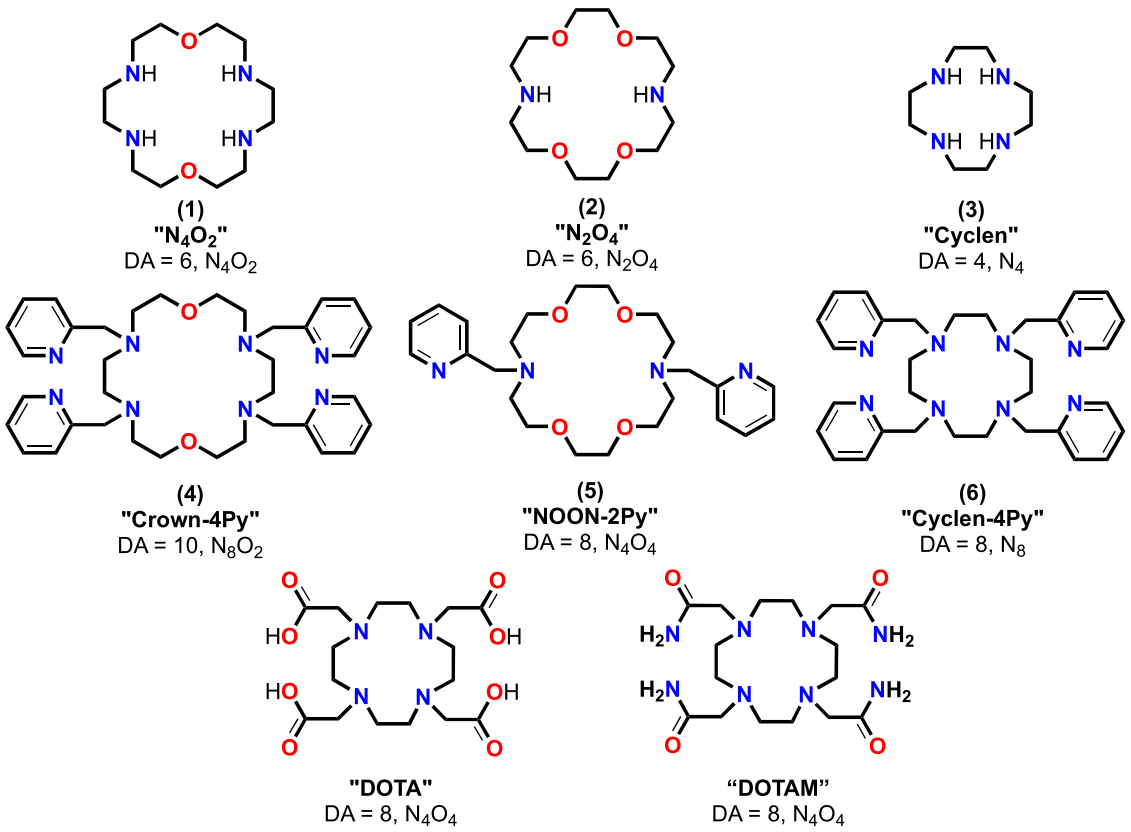

Figure 1. Core macrocyclic structures (top row), macrocyclic pyridyl-containing chelators (middle row), and commercially available chelators of interest (bottom row) investigated in this study. DA = donor atoms.

To realize the full potential of *theranostic* radiopharmaceuticals, the biodistribution and chemical properties of the isotope pair being used must be very similar, if not identical. If the biodistribution of the imaging radiopharmaceutical differs greatly from the therapeutic, an inappropriate treatment method may be chosen with which there can be adverse effects.[3] Chemically matched, or element-equivalent, theranostic isotope pairs, which are composed of isotopes of the same element, are ideal as the chemical properties of the isotopes are essentially identical and thus should have identical biodistribution.[4,5] In this regard, lead-203 (^{203}Pb, $t_{1/2}$ = 51.9 h) and lead-212 (^{212}Pb, $t_{1/2}$ = 10.6 h) are a promising element-equivalent theranostic pair that is currently being explored for clinical use.[6] ^{203}Pb decays via electron capture and releases a 279 keV photon with an abundance of 81%, making it compatible with SPECT imaging. ^{212}Pb emits both β- and α-particles (via its daughter ^{212}Bi), making it compatible with therapy.

Diagnostic and therapeutic radiopharmaceuticals utilizing matched theranostic pairs can have nearly identical biodistribution as they are able to utilize identical bioconjugates (chelate−linker−targeting vector) for radiometal chelation because both radioisotopes are the same element and will thus share identical coordination properties. This results in the same molecular properties such as overall charge, hydrophilicity, and same chemical properties for both imaging and therapeutic drug forms. In addition, the thermodynamic stability of the complex and its kinetic inertness are critical to the success of the BFC approach. Chelates can have a significant effect on the pharmacokinetic properties of a radiopharmaceutical, and for one to be effective at coordinating and containing the radiometal, its design must be tailored to the metal's chemical properties.[7,8] In general, there are two broad chelator categories: acyclic and macrocyclic, both of which have two main components: (i) a backbone that serves as an anchor to connect (ii) pendant functional arms containing electron-donor moieties for metal coordination. Macrocyclic chelators have constricted geometries as their rigid backbones form a pre-organized metal ion-binding site resulting in a decreased entropic penalty and thus an increased thermodynamic favorability toward complexation when compared to their acyclic counterparts.[9] This phenomenon is commonly referred to as the macrocycle effect.[9] However, macrocycles tend to have slower reaction kinetics requiring elevated temperatures to induce complexation, which can be detrimental when handling a heat- or pH-sensitive targeting vector and thus the choice of chelator type can depend on the reaction environment.[8]

The choice of chelating moieties is often based on the hard−soft acid−base (HSAB) theory, which matches harder (nonpolarizable) acids with harder bases and softer (more-polarizable) acids with softer bases to result in the most stable coordination complexes.[10−12] Pb^{2+} is considered an intermediate Lewis acid and thus should form the most stable complexes with intermediate Lewis bases, including pyridine and amides. For example, the structure of the current commercial standard for lead chelation, DOTAM, also known as TCMC (1,4,7,10-tetrakis(carbamoylmethyl)-1,4,7,10-tetraazacyclododecane), employs four pendant amides where the carbonyl oxygen acts as an electron donor.[11,13]

In addition to the choice of donor moieties, the macrocyclic ring size can greatly affect complex stability and metal

https://doi.org/10.1021/acs.inorgchem.2c01114
Inorg. Chem. 2022, 61, 9638−9649

selectivity.[9] Crown- and aza-crown ethers are attractive backbones for the design of macrocyclic chelators for radiopharmaceuticals due to their ease of functionalization and a wide variety of potential ring sizes. With a judicious choice of donor atoms and ring size, one can design macrocyclic chelates with enhanced selectivity toward specific metals. Despite this, the understanding of the relationship between structure, metal selectivity, and complex stability is often limited to the idea of size-match selectivity, although this has been contested.[9] However, these trends often do not translate when donor arms are introduced and can be unpredictable, especially with bulky donor groups, like pyridine, where steric strain can have a large role in complex formation;[9] thus, these relationships should be studied on a case-by-case basis. A further understanding of this relationship can advance not only metal-based radiopharmaceutical development but also the design of antibiotics,[14] ion-exchange resins,[15] and metal intoxication treatments,[16] among others.

The focus of this study is to investigate the effect of macrocyclic backbone size in pyridyl-containing chelators to identify optimal chelators for $[^{203/212}Pb]Pb^{2+}$ radiopharmaceuticals. The optimal chelator will complex ^{203}Pb at a low chelator:metal ratio with fast kinetics and be thermodynamically stable and kinetically inert to prevent transchelation with endogenous metal-seeking biomolecules *in vivo*. We hypothesized pyridyl, an intermediate Lewis base, will form stable complexes with Pb^{2+}, an intermediate Lewis acid. The outcome of this study provides insights into the ideal backbone size required for minimal steric strain, which should increase the thermodynamic favorability of complexation and be reflected by higher radio-lead incorporation yields. Results of concentration-dependent ^{203}Pb radiolabeling, kinetic inertness, and serum stability studies with a panel of pyridyl-containing chelators have been rationalized based on the solid-state Pb-complex structures (elucidated via X-ray diffraction), solution structures (via ^1H nuclear magnetic resonance (NMR) spectroscopy), and thermodynamic stability constants (determined via potentiometric titrations). The pyridyl-containing chelators and commercial standards investigated in this study are shown in Figure 1. The 18-membered macrocycles, NOON-2Py (7,16-bis(pyridin-2-ylmethyl)-1,4,10,13-tetraoxa-7,16-diazacyclooctadecane) and crown-4Py (4,7,13,16-tetrakis-(pyridin-2-ylmethyl)-1,10-dioxa-4,7,13,16-tetraazacyclooctadecane), have been investigated previously for use as a lead detoxifying agent[17] and as a biomimetic model of the methane monooxygenase enzyme for alkane functionalization when complexed to manganese,[18] respectively. The 12-membered macrocycle cyclen-4Py (1,4,7,10-tetrakis(pyridin-2-ylmethyl)-1,4,7,10-tetraazacyclododecane) was synthesized previously to investigate its coordination of copper, bismuth, and lanthanum.[19−22] These pyridyl-containing macrocycles were compared to commercial standard chelators DOTAM and DOTA (1,4,7,10-tetraazacyclododecane-1,4,7,10-tetraacetic acid).

EXPERIMENTAL SECTION

General. All chemicals were purchased from commercial suppliers and used without further purification. The 18-membered backbone, 1,10-dioxa-4,7,13,16-tetraazacyclooctadecane (N_4O_2, (**1**)), was synthesized as previously described with no deviations.[23] The 18-membered backbone, 1,4,10,13-tetraoxa-7,16-diazacyclooctadecane (N_2O_4, (**2**)), was purchased from VWR (Radnor, PA). The backbone, 1,4,7,10-tetraazacyclododecane (Cyclen, (**3**)), was purchased from TCI. Commercial chelators, DOTA (1,4,7,10-Tetraazacyclododecane-1,4,7,10-tetraacetic acid) and DOTAM (1,4,7,10-Tetrakis-(carbamoylmethyl)-1,4,7,10-tetraazacyclododecane), were purchased from Macrocyclics Inc. (Plano, TX). Anhydrous solvents were obtained following storage over 3 Å molecular sieves activated under heat. Water was purified using a MilliQ purification system. NMR spectra were obtained using a Bruker 400 (400 MHz), Bruker 500 (500 MHz), or a Bruker 600 (600 MHz) (Billerica, MA) with signals measured relative to the signal of the solvent. Mass spectrometry was performed using either an Agilent (Santa Clara, CA) 6210 TOF LC/MS or Advion expression LC-MS (Ithaca, NY) equipped with an electrospray source. The ^{203}Pb utilized for radiolabeling studies was produced as previously described and received as $[^{203}Pb]Pb(OAc)_2$ in 1 M ammonium acetate (NH_4OAc).[24] Quantification of ^{203}Pb activity per reaction was quantified using γ ray spectroscopy on an N-type co-axial high-purity germanium (HPGe) γ spectrometer from Canberra Industries (Meridan, CT). The γ spectrometer was calibrated with a 20 mL ^{152}Eu and ^{133}Ba source.

Chelator Synthesis. The synthetic scheme can be found in the supporting information (Scheme S1).

General procedure. To a stirred suspension of the respective macrocyclic backbone (1 equiv) and K_2CO_3 (5 equiv) in 10 mL of anhydrous acetonitrile, a 10 mL solution of 2-(bromomethyl)pyridine hydrobromide (4.5 equiv) was added dropwise at room temperature over the course of 10 min and left to react for 48 h. After 48 h, the K_2CO_3 was filtered off and the solvent was removed by rotary evaporation. The crude red oil was redissolved in dichloromethane and washed at least three times, or until the aqueous phase was no longer pink, with equal volumes of saturated sodium bicarbonate. The organic layers were combined, and the solvent was removed by rotary evaporation. Further purification, if necessary, as determined by the quality of the ^1H NMR spectrum, is described below.

*4,7,13,16-tetrakis(pyridin-2-ylmethyl)-1,10-dioxa-4,7,13,16-tetraazacyclooctadecane (Crown-4Py, (**4**)).* The recovered oil was further purified by reverse-phase semipreparative high-performance liquid chromatography using a Phenomenex Luna C18 (250 mm × 100 mm) column at 3 mL/min with the following method: A: H_2O with 0.1% TFA, B: Acetonitrile (CH_3CN) with 0.1% TFA; 0−5 min 10% B; 5−20 min 10−100% B, 20−25 min 100% B. The fraction at 11.8 min was collected and lyophilized to yield crown-4Py as a yellow powder (56.9 mg, 48%). ^1H NMR (500 MHz, CD_2Cl_2) δ 8.44 (d, J = 4.76 Hz, 4H), 7.58 (td, J = 7.7, 1.8 Hz, 4 H), 7.46 (d, J = 7.83 Hz, 4 H), 7.11 (m, 4H), 3.72 (s, 8 H), 3.53 (t, J = 5.6 Hz, 8 H), 2.79 (s, 8 H), 2.77 (t, J = 5.8 Hz, 8 H). ^{13}C NMR (125 MHz, CD_2Cl_2) δ 160.6, 148.7, 136.1, 122.7, 121.6, 69.92, 61.49, 53.2. HR-MS calcd for $[C_{36}H_{48}N_8O_2 + H]^+$: 625.3978; found, 625.3979.

*7,16-bis(pyridin-2-ylmethyl)-1,4,10,13-tetraoxa-7,16-diazacyclooctadecane (NOON-2Py, (**5**)).* Further purification by HPLC was not required and so a light-yellow powder was yielded (103.0 mg, 61% yield). ^1H NMR (400 MHz, CD_2Cl_2) δ 8.47 (d, J = 5.0 Hz, 2 H), 7.64 (dd, J = 7.8, 1.8 Hz, 2 H), 7.53 (d, J = 7.7 Hz, 2 H), 7.13 (dd, J = 7.1, 5.1 Hz, 2 H), 3.80 (s, 4 H), 3.59 (t, J = 5.8 Hz, 8 H), 3.56 (s, 8 H), 2.82 (t, J = 5.8 Hz, 8 H). ^{13}C NMR (100 MHz, DMSO-d_6) δ 159.9, 148.8, 136.6, 122.8, 122.1, 69.8, 69.0, 60.9, 53.9. HR-MS calcd for $[C_{24}H_{36}N_4O_4 + H]^+$: 445.2815; found 445.2824.

*1,4,7,10-tetrakis(pyridin-2-ylmethyl)-1,4,7,10-tetraazacyclododecane (Cyclen-4Py, (**6**)).* The recovered oil was further purified by reverse-phase semipreparative high-performance liquid chromatography using a Phenomenex Luna C18 (250 mm × 100 mm) column at 3 mL/min with the following method: A: H_2O with 0.1% TFA, B: Acetonitrile (CH_3CN) with 0.1% TFA; 0−5 min 10% B; 5−20 min 10−100% B, 20−25 min 100% B. The fraction at 12.6 min was collected and lyophilized to yield cyclen-4Py as a light-yellow powder (322.5 mg, 69%). ^1H NMR (400 MHz, CD_3CN) δ 8.35 (d, J = 5.1 Hz, 4H), 7.87 (td, J = 7.8, 1.8 Hz, 4H), 7.47 (d, J = 1.2 Hz, 4H), 7.41 (m, 4H), 4.30 (s, 8H), 3.33 (s, 16H). ^{13}C NMR (100 MHz, CD_3CN) δ 151.63, 147.81, 139.47, 125.07, 124.43, 56.20, 49.47. HR-MS calcd for $[C_{32}H_{40}N_8 + H]^+$: 537.3454; found, 537.3450.

Synthesis of Pb Complexes. **Caution: Perchlorate salts are considered potentially explosive and should be handled with care.

https://doi.org/10.1021/acs.inorgchem.2c01114
Inorg. Chem. 2022, 61, 9638−9649

[Pb(Cyclen-4Py)]$^{2+}$. To a solution of cyclen-4Py in methanol (1 mL, 22.4 mg, 41.7 μmol), a methanolic solution of $Pb(ClO_4)_2{\cdot}3H_2O$ (19.2 mg, 41.7 μmol) was added. A yellow solid immediately precipitated out of solution. The solid was placed in a centrifuge at 10,000 rpm for 2 min, and the supernatant was removed. This process was repeated 3 times (3 × 500 μL) with methanol, followed by washing with diethyl ether (3 × 500 μL) before drying under vacuum (18.3 mg, 59.0%). An aliquot was taken for NMR studies and dissolved in deuterated acetonitrile. The complex was redissolved in dimethylformamide (1 mL), and via vapor diffusion of tetrahydrofuran, single crystals suitable for X-ray diffraction analyses were obtained. ^{1}H NMR (500 MHz, CD_3CN) δ 7.90 (s, 4H), 7.65 (s, 4H), 7.42 (d, J = 7.7 Hz, 4H), 7.25 (s, 4H), 4.19 (d, J = 15.9 Hz, 4H), 4.01 (d, J = 15.5 Hz, 4H), 3.55 (t, J = 14.1 Hz, 4H), 3.09 (t, J = 13.8 Hz, 4 H), 2.80 (m, 8 H). NMR spectrum found in supplementary information (Figures S7−10) HR-MS calcd for $[C_{32}H_{40}N_8 + Pb]^{2+}$: 372.1571; found, 372.1578.

[Pb(Crown-4Py)]$^{2+}$. To a solution of crown-4Py in methanol (1 mL, 15.2 mg, 24.3 μmol), a methanolic solution of $Pb(ClO_4)_2{\cdot}3\ H_2O$ (11.2 mg 24.3 μmol) was added. Immediately, a yellow solid precipitated out of solution. The washing procedure for this solid was identical to that described for $[Pb(Cyclen\text{-}4Py)]^{2+}$, and the solid was dried under vacuum (20.2 mg, 99.0%). An aliquot was taken for NMR studies and dissolved in deuterated acetonitrile. The complex was redissolved in acetonitrile (1 mL), and via vapor diffusion of diethyl ether, single crystals suitable for X-ray diffraction analyses were obtained. Multiple isomers were found in solution. The NMR spectrum is found in the supplementary information (Figures S11−14). HR-MS cald for $[C_{36}H_{48}N_8O_2 + Pb]^{2+}$: 416.1834; found 416.1834.

[Pb(NOON-2Py)]$^{2+}$. To a solution of NOON-2Py in methanol (1 mL, 24.4 mg, 54.39 μmol), a methanolic solution of $Pb(ClO_4)_2{\cdot}3\ H_2O$ (27.5 mg 59.8 μmol) was added. Unlike the previous two complexes, a solid did not precipitate. To this, a solution of NH_4PF_6 (21.1 mg, 129.5 μmol) in deionized water was added to exchange the perchlorate counterions for hexafluorophosphate as numerous attempts to form crystals with the perchlorate counterion failed. The solvent was removed under a steady stream of nitrogen to give a pale yellow solid, which was washed 3 times with diethyl ether and then dried under vacuum (17.8 mg, 50.2%). An aliquot was taken for NMR studies and dissolved in deuterated DMSO. The complex was redissolved in dimethylformamide (1 mL), and via vapor diffusion of tetrahydrofuran, single crystals suitable for X-ray diffraction analyses were obtained. Multiple isomers were found in solution. The NMR spectrum is found in the supplementary information (Figures S15−18). HR-MS cald for $[C_{24}H_{36}N_4O_4$ + acetate $(C_2H_3O_2)$ + $Pb]^+$: 711.2641; found 711.2638.

X-ray Crystallography. All crystals were mounted on a 150 mm MiTeGen Dual-Thickness MicroMount using Paratone oil, and measurements were made on a Bruker Photon II diffractometer with TRIUMPH-monochromated Mo Kα radiation (sealed tube) or Cu Kα radiation (Cu-microsource). The data were collected at a temperature of 298 K in a series of scans in 0.50° oscillations. Data were collected and integrated using the Bruker SAINT software package (Version 7.46A) and were corrected for absorption effects using the multiscan technique (SADABS) or (TWINABS). All structures were solved by direct methods.[25,26] All nonhydrogen atoms were refined anisotropically. All hydrogen atoms were placed in calculated positions but not refined. All refinements were performed using the SHELXTL crystallographic software package of Bruker-AXS (Version 5.1). The molecular drawings were generated by the use of POV.[27] Additional crystallographic information can be found in the Supplemental Information.

pH Potentiometry. Potentiometric titrations were carried out using a Metrohm Titrando 888 titrator controlled by *Tiamo 2.5* software and equipped with a Ross Orion combination electrode (8103BN, ThermoFisher Scientific) and a Metrohm 806 exchange unit with an automatic burette (10 mL). The titration vessel was fitted into a removable glass cell (≈70 mL) maintained at 25 °C (pK_w = 13.78)[28] using a Thermomix 1442D circulating water bath. CO_2 was excluded from the setup using a positive pressure of argon, which was passed through an aqueous 30 wt % KOH solution. Aqueous KOH (0.1 M, BDH Chemicals, Radnor, PA) and aqueous HCl (0.1 M, J.T. Baker, Phillipsburg, NJ) commercially obtained were standardized by potentiometric titration against potassium hydrogen phthalate or TRIS base, respectively. The glass electrode was calibrated before each titration by titrating a solution of standardized HCl (5 or 10 mM) with standardized KOH. The data were analyzed using the program *Glee*[29] (version 3.0.21) to obtain the standard electrode potential, slope, and slope factor. The ionic strength of the titration solutions was maintained at 0.1 M using KCl (>99.5%, BioUltra, Sigma-Aldrich), and the titration solutions were allowed to equilibrate for 15 min prior to addition of the titrant. Ligand stock solutions were prepared by dissolving HCl salts of the ligands in pure water, and their exact concentrations were determined based on the end points of the potentiometric titration curves obtained during the protonation constant measurements. Inductively coupled plasma (ICP) standard solutions (VWR BDH Aristar) of lead (10,000 μg/mL) in nitric acid (0.5% v/v) were employed as the source of metal ions in the titrations.

Protonation constant measurements were carried out by titrating an aqueous solution (∼15 mL) of a free ligand (∼1 mM) and HCl (∼10 mM) with standardized KOH (0.1 M). The ionic strength of the solution was maintained at 0.1 M using KCl. The titration method employed a 0.1 mV/min drift limit with a minimum and maximum wait time of 0 s and 180 s, respectively, between addition of KOH aliquots (0.020 mL volume increments). The titration data within the pH range of 2.2−11.3 were analyzed using *Hyperquad2013* software.[30] The protonation constants were calculated from the average of three independent titrations. Stability constant measurements were carried out by titrating an aqueous solution (∼15 mL) of the ligand (∼1 mM), metal (∼1 mM), and HCl (∼10 mM) with standardized KOH (0.1 M). The ionic strength of the solution was maintained at 0.1 M using KCl. The titration method employed a 0.1 mV/min drift limit with a minimum and maximum wait time of 0 s and 300 s, respectively, between addition of KOH aliquots (0.015 mL volume increments). No metal hydroxide precipitation was observed within the pH range and concentration employed. The titration data within the pH range of 2.2−11.3 were analyzed using *Hyperquad2013* software. The stability constants were calculated from the average of three independent titrations.

Radiolabeling. **Caution: ^{203}Pb emits ionizing radiation and should only be used in a facility designed in accordance with appropriate safety controls.

The chelators DOTA, DOTAM, crown-4Py, NOON-2Py, and cyclen-4Py were dissolved in deionized water to give 10^{-3} M stock solutions from which serial dilution was used to prepare chelator solutions from 10^{-4} to 10^{-6} M. A 10 μL aliquot of the respective chelator, or deionized water as a negative control, was further diluted with 80 μL of deionized water, and for ^{203}Pb labeling studies, $[^{203}Pb]Pb(OAc)_2$ (85 kBq, 10 μL, 1 M NH_4OAc, pH 7) was added and mixed at ambient temperature to begin the reaction. The instant thin layer chromatography (iTLC) plate system used to separate the "free/uncomplexed" ^{203}Pb from the complexed ^{203}Pb was iTLC-SA (iTLC paper impregnated with silicic acid) plates (1.5 × 10 cm, baseline at 1.5 cm; Agilent Technologies) developed with 50 mM EDTA (pH 5.0). With this system, the complexed $^{203}Pb^{2+}$ remained at the baseline (R_f = 0) and the free $^{203}Pb^{2+}$ migrated with the solvent front ($R_f \sim 1$). At 60 min, 10 μL aliquots were spotted onto the plates and developed. Once dried, radiochemical yields (RCYs) were measured using a BioScan System 200 Scanner (Washington, DC) and quantified with WinScan software.

Human Serum Stability. The serum stabilities of the $[^{203}Pb^{2+}]$-$[Pb(DOTA)]^{2-}$ and $[^{203}Pb^{2+}][Pb(DOTAM)]^{2+}$ complexes were previously evaluated.[24] To perform serum stability studies with the cyclen-4Py complex, a 10 μL aliquot of the 10^{-4} M chelator solution was added to 80 μL of deionized water and 10 μL of $[^{203}Pb]Pb$-$(OAc)_2$ (85 kBq,1 M NH_4OAc, pH 7). To ensure prior to the start of the study that the RCY was 100%, a 10 μL aliquot was removed at 60 min. Once a quantitative yield was confirmed as previously described,

https://doi.org/10.1021/acs.inorgchem.2c01114
Inorg. Chem. 2022, 61, 9638−9649

Table 1. Relevant Crown Ether Cavity and Pb^{2+} Ionic Radii

Crown ether	Cavity size[32]	Pb^{2+} CN	Pb^{2+} ionic radius[33]
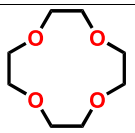 12-crown-4	r = 0.6 – 0.75 Å d = 1.2 – 1.5 Å	4	0.98
		6	1.19
		7	1.23
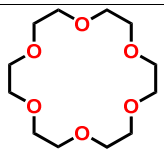 18-crown-6	r = 1.3 – 1.6 Å d = 2.6 – 3.2 Å	8	1.29
		9	1.35
		10	1.40

human serum (90 μL) was added and incubated at 37 °C. At 24, 48, and 72 h time points, an aliquot (10 μL) of the mixture was removed and spotted onto the iTLC-SA plates, developed, and measured as previously described to determine the amount of the complex intact.

EDTA and Pb Challenge Studies. A stock solution of 20 mM ethylenediaminetetraacetic acid (EDTA) was prepared in H_2O, and the pH was adjusted to 7.0 using aqueous sodium hydroxide. A stock solution of 20 mM lead (II) acetate was prepared in H_2O. Preformed $[^{203}Pb]Pb^{2+}$ complexes, prepared as described above at a chelator concentration of 10^{-4} M and RCY >99% after 1 h post ^{203}Pb addition at ambient temperature, were challenged with 20-fold excess EDTA or nonradioactive Pb. To the complex solution, an aliquot (10 μL) of the EDTA or Pb solution was added. At 0.5, 24, 48, and 72 h time points, an aliquot (10 μL) of the mixture was removed and spotted onto the iTLC-SA plates, developed, and measured as previously described to evaluate the kinetic inertness of the complex.

RESULTS AND DISCUSSION

Depending on the radius of the metal cation and macrocycle cavity, three main types of complexes are formed.[31,32] If the metal cation is of an appropriate size to fit within the cavity, encapsulating meridional complexes typically result.[31] If the metal cation is too large to be encapsulated, the metal will sit above the cavity and form either a facial or sandwich complex; with facial complexes forming when the metal is coordinated above the cavity of a single chelator, while sandwich complexes occur when a single metal atom is complexed between two individual chelators.[31] The radii of the cavity of relevant crown ethers in this study and Pb^{2+} ionic radii as a function of coordination number (CN) are listed in Table 1.

Although the structures shown in Table 1 are of the oxygen-rich crown ethers, the radii of the aza-derivatives of interest to this study should be nearly equivalent as the covalent radii of oxygen and nitrogen are 0.66 Å and 0.70 Å, respectively.[34] From this table, one can observe that with a CN of 8, the maximum potential CN found in cyclen-4Py, with an ionic radius of 1.29 Å, Pb^{2+} is too large to form meridional complexes with the chelator and thus should form a facial complex where the Pb^{2+} sits above the cavity. With crown-4Py and a possible maximum CN of 10, with an ionic radius of 1.40 Å, the Pb^{2+} should be fully encapsulated in a meridional complex.

With these two pyridyl-containing chelators expected to form two different types of complexes with Pb^{2+} due to their backbone size, the effect of the size difference of these macrocycles on their radiolabeling ability was investigated. The ^{203}Pb radiolabeling was performed in 0.1 M NH_4OAc at pH 7 and at ambient temperatures, as these mild conditions are ideal when working with heat-sensitive biomolecules, including antibodies. The RCYs were compared to that of DOTA and DOTAM, both commercially available standards, with DOTAM being widely regarded as the gold standard for lead chelation. Our initial hypothesis was that crown-4Py would have superior selectivity and metal incorporation ability, and therefore greater RCYs, over cyclen-4Py due to the larger and more similar cavity size of the former when compared to the ionic radius of Pb^{2+}.

A summary of RCYs is illustrated in Figure 2. The RCYs for crown-4Py at concentrations between 10^{-4} and 10^{-7} M were

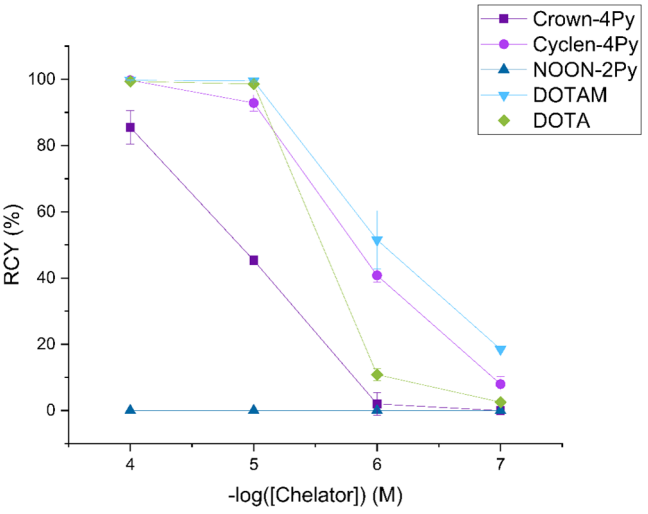

Figure 2. Radiochemical yields (RCYs, %) for ^{203}Pb radiolabeling reactions (conditions = 1 h, ambient temperature, and chelator concentrations between 10^{-4} and 10^{-7} M) (n = 3 each data point).

85.5 ± 5.0, 45.3 ± 1.4, 2.0 ± 3.5, and 0%, respectively. RCYs for cyclen-4Py at the same concentrations were 99.7 ± 0.2, 92.8 ± 2.5, 40.8 ± 2.0, and 8.0 ± 2.3%, respectively. For DOTA, the RCYs were 99.4 ± 0.4, 98.6 ± 0.3, 10.8 ± 1.8, and 2.5 ± 0.3%, respectively. For the commercial standard DOTAM, RCYs of 99.7 ± 0.2, 99.5 ± 0.4, 51.5 ± 8.8, and 18.5 ± 0.1% were observed. Although it was unsurprising that DOTAM demonstrated the highest RCYs, what was surprising was the overall low yields for crown-4Py based on our initial hypothesis. At no concentration tested was the yield quantitative, making it difficult to justify pursuing this chelator in a clinical setting for either ^{203}Pb or ^{212}Pb. Serum stability, EDTA challenge, and nonradioactive Pb^{2+} challenge studies

https://doi.org/10.1021/acs.inorgchem.2c01114
Inorg. Chem. 2022, 61, 9638−9649

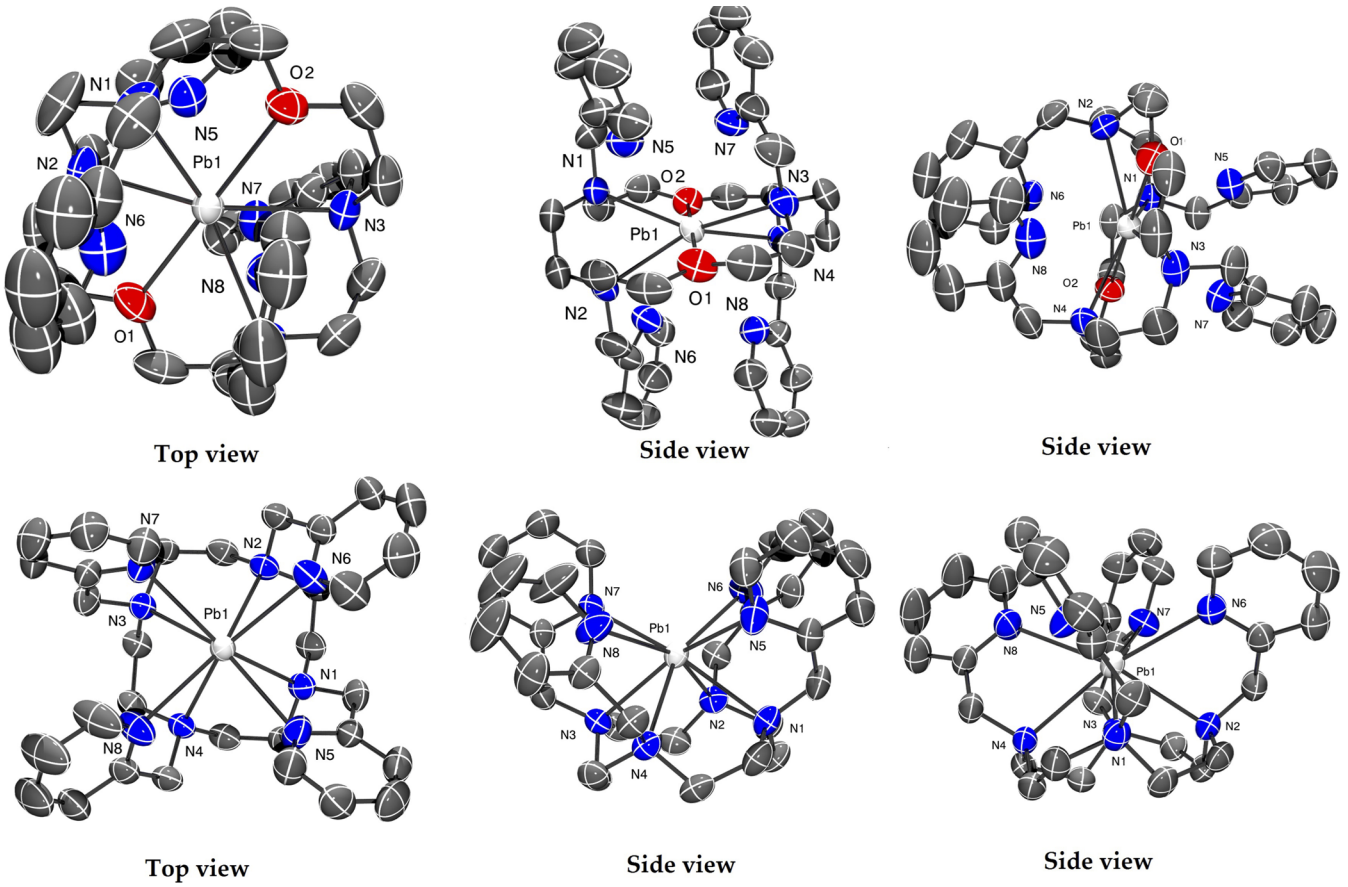

Figure 3. X-ray crystal structures of $[Pb(Crown\text{-}4Py)]^{2+}$ (top) and $[Pb(Cyclen\text{-}4Py)]^{2+}$ (bottom) complexes with labeled atoms; hydrogen atoms and counter anions were omitted for clarity. Ellipsoids drawn at the 50% probability level.

with cyclen-4Py showed that after 72 h, 97.0 ± 2.8, 98.1 ± 0.5, and 98.0 ± 0.4% of the complex remained intact, respectively, indicating that $[^{203}Pb][Pb(cyclen\text{-}4Py)]^{2+}$ is a highly inert complex compatible with radiopharmaceutical applications (Tables S1−S3).

Aiming to rationalize the RCYs and understand the structure-radiolabeling ability relationship of Pb^{2+}-chelators with bulky pyridyl donor groups, the complexes were also studied by ^{1}H NMR, X-ray diffraction, and potentiometry to determine the thermodynamic stability and protonation constants. The ability to study Pb complexes with these techniques is another benefit of this theranostic pair as, unlike an emerging α-emitter, actinium-225 (^{225}Ac), stable isotopes of this element exist, including ^{207}Pb, which is NMR active.

The solid-state structures of the Pb^{2+} complexes of cyclen-4Py and crown-4Py, shown in Figure 3, as well as the Pb^{2+} complexes of their respective cyclen and N_4O_2 backbones (Figure S19), were determined by X-ray diffraction. Select interatomic distances and angles of the metal coordination environment are given in Tables 2 and 3, respectively.

As shown in the crystal structure, the crown-4Py complex presents a staggered conformation with adjacent pyridyl groups nearly 180° to each other, while the Pb^{2+} complex of cyclen-4Py presents a *syn* conformation with all four of the pyridyl arms on the same side of the complex. As expected, crown-4Py formed a meridional complex with Pb^{2+} coordinated within the ring and cyclen-4Py formed a facial complex with the Pb^{2+} situated above the ring.

Table 2. Select Interatomic Distances (Å) in the Metal Coordination Environment in $[Pb(Cyclen\text{-}4Py)]^{2+}$ and $[Pb(Crown\text{-}4Py)]^{2+}$ Complexes

	$[Pb(Cyclen\text{-}4Py)]^{2+}$	$[Pb(Crown\text{-}4Py)]^{2+}$
Pb(1)−N(1)	2.630(2)	2.806(3)
Pb(1)−N(2)	2.652(2)	2.769(3)
Pb(1)−O(1)	n/a	2.613(3)
Pb(1)−O(2)	n/a	2.604(3)
Pb(1)−N(5)	2.712(3)	3.113
Pb(1)−N(6)	2.776(3)	2.995
Pb(1)−N(7)	2.781(2)	2.924
Pb(1)−N(8)	2.823(2)	3.026

Table 3. Select N−Pb−N Bond Angles (°) in the Metal Coordination Environment in $[Pb(Cyclen\text{-}4Py)]^{2+}$ and $[Pb(Crown\text{-}4Py)]^{2+}$ Complexes

	$[Pb(Cyclen\text{-}4Py)]^{2+}$	$[Pb(Crown\text{-}4Py)]^{2+}$
N(1)−Pb(1)−N(5)	63.14(8)	55.8(1)
N(2)−Pb(1)−N(6)	64.10(8)	56.72(9)
N(3)−Pb(1)−N(7)	60.90(7)	58.0(1)
N(4)−Pb(1)−N(8)	63.41(7)	57.10(9)
N(1)−Pb(1)−N(4)	68.95(7)	n/a
N(2)−Pb(1)−N(3)	69.55(7)	n/a
N(1)−Pb(1)−N(2)	68.87(7)	66.8(1)
N(3)−Pb(1)−N(4)	67.74(7)	67.05(9)

The maximum interatomic distance for a Pb−N interaction to be considered coordinating is approximately 2.9 Å.[33] In each

https://doi.org/10.1021/acs.inorgchem.2c01114
Inorg. Chem. 2022, 61, 9638−9649

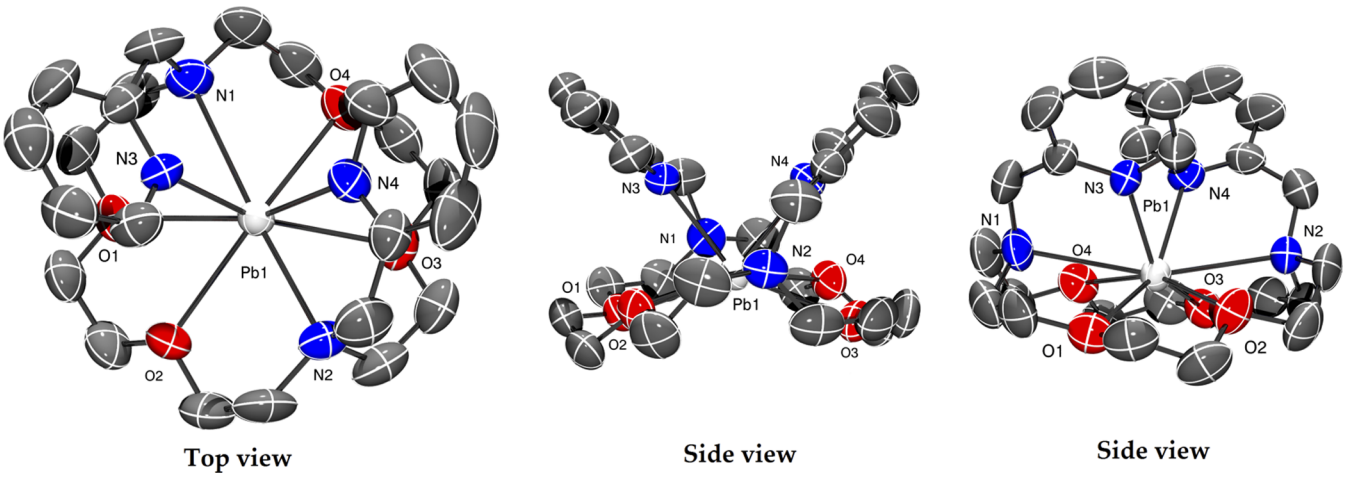

Figure 4. X-ray crystal structure of the $[Pb(NOON\text{-}2Py)]^{2+}$ complex with labeled atoms; hydrogens and counter anions were omitted for clarity. Ellipsoids are drawn at the 50% probability level.

of the complexes, both the Pb−O and Pb−N bonds in the macrocyclic backbone meet this requirement. The shorter average Pb−O interatomic distance (2.609(3) Å) in the crown-4Py N_4O_2 backbone is reflective of the harder nature of the oxygen donor compared to its nitrogen counterpart, with an average backbone Pb−N interatomic distance of 2.770(3) Å. Interestingly, the Pb−N bonds in the cyclen-4Py backbone exhibited an average distance of 2.641(2) Å, while the average $Pb-N_{pyr}$ (pyridine group nitrogen) distance was 2.773(3) Å; both were substantially shorter than the same associations observed in the crown-4Py complex, which maintained an average interatomic distance of 3.015 Å. With Pb^{2+} sitting deeper in the macrocyclic cavity of crown-4Py, this likely negatively affects the accessibility of the lead ion by the pyridine nitrogen atoms, resulting in longer associations that make coordination less favorable by these bulky donor groups and potentially explaining the lower radiochemical yields. With Pb^{2+} coordinated to cyclen-4Py in an exocyclic manner, the Pb^{2+} sits above the cyclen backbone, making it more accessible to the bulkier pyridyl groups.

The thermodynamic favorability of cyclen-4Py over crown-4Py Pb-complex formation is further evinced by the bond angles observed in the five-membered ring, which form between the backbone nitrogen atoms, lead, and pyridine nitrogens ($N-Pb-N_{pyr}$). These angles are summarized in Table 3. To reduce steric strain and consequently increase thermodynamic favorability, the ideal bond angle of these five-membered rings should be ∼69°, any deviation from this suggests an increase in steric strain.[35] The average $N-Pb-N_{pyr}$ bond angles for $[Pb(Crown\text{-}4Py)]^{2+}$ and $[Pb(Cyclen\text{-}4Py)]^{2+}$ are 56.91 and 62.90°, respectively. The larger deviation from the ideal bond angle in the crown-4Py complex (∼12°) compared to the cyclen-4Py complex (∼7°) indicates a larger strain energy in the former compared to the latter, reducing the Pb-complex thermodynamic favorability and potentially explaining crown-4Py's poor metal incorporation ability.

Given the inability of the four pyridyl groups to coordinate Pb in the crown-4Py complex, it was hypothesized that reducing the number of pyridyl groups from four to two would reduce both steric strain and the loss of entropy the chelator experiences during complex formation. As such, the 18-membered N_2O_4 backbone chelator NOON-2Py (Figure 1) was studied. This backbone cavity still possesses approximately the same diameter as Pb^{2+} at a coordination number of 8, presumably conserving size selectivity. Surprisingly, macrocyclic NOON-2Py was not able to incorporate the radio-lead under any condition tested. Investigation into the coordination chemistry was also performed with X-ray diffraction studies, with the crystal structure shown in Figure 4.

In literature, steric strain is minimized when the lone pairs of nitrogen atoms in a five-membered coordination ring are situated so as to produce a M−N association distance of 2.5 Å.[35] For $[Pb(NOON\text{-}2Py)]^{2+}$, it was found that the average $Pb-N_{pyr}$ interatomic distance was 2.587(4) Å and the average $N-Pb-N_{pyr}$ angle was 65.0(1)°, the closest of all of the macrocyclic pyridyl chelators investigated to the ideal literature values, which should suggest that there is minimal steric strain energy involved in complexation. On this basis alone, one would have expected NOON-2Py to give rise to the highest ^{203}Pb incorporation yields; however, no incorporation was observed. Given these results, other aspects of the structure as well as the difference between experiments performed at the tracer level versus the macroscopic scale must be considered to provide insight into these results.

Due to its electron configuration of $[Xe]4f^{14}5d^{10}6s^2$, Pb^{2+} exhibits an inert-pair effect as the outermost electrons of Pb^{2+} are not involved in bond formation.[36] This inert lone pair of electrons can thus cause a nonspherical distribution of the donating electrons around the Pb^{2+} and, depending on the chelator, can form a distinct void in the coordination sphere.[36] In this situation, the lone pair is designated as stereochemically active with this type of geometry referred to as hemidirected.[36] When the donating arms are located evenly throughout the coordination sphere, it is referred to as holodirected coordination.[36] The nature of the coordination is determined heavily by the coordination number and geometry of the chelator itself. With CN from 2−5, all complex geometries are hemidirected and from 9−10, all are holodirected, but from 6−8, both geometries are possible.

With a possible CN of 8 for NOON-2Py, holo- or hemidirected coordination is possible for $[Pb(NOON\text{-}2Py)]^{2+}$. With both pyridyl groups located on the same side of the complex, it takes on a *syn*-like conformation. This *syn*-like conformation may be due to the presence of a stereochemically active lone pair that results in hemidirected geometry, causing a large void in the coordination sphere. A

https://doi.org/10.1021/acs.inorgchem.2c01114
Inorg. Chem. 2022, 61, 9638−9649

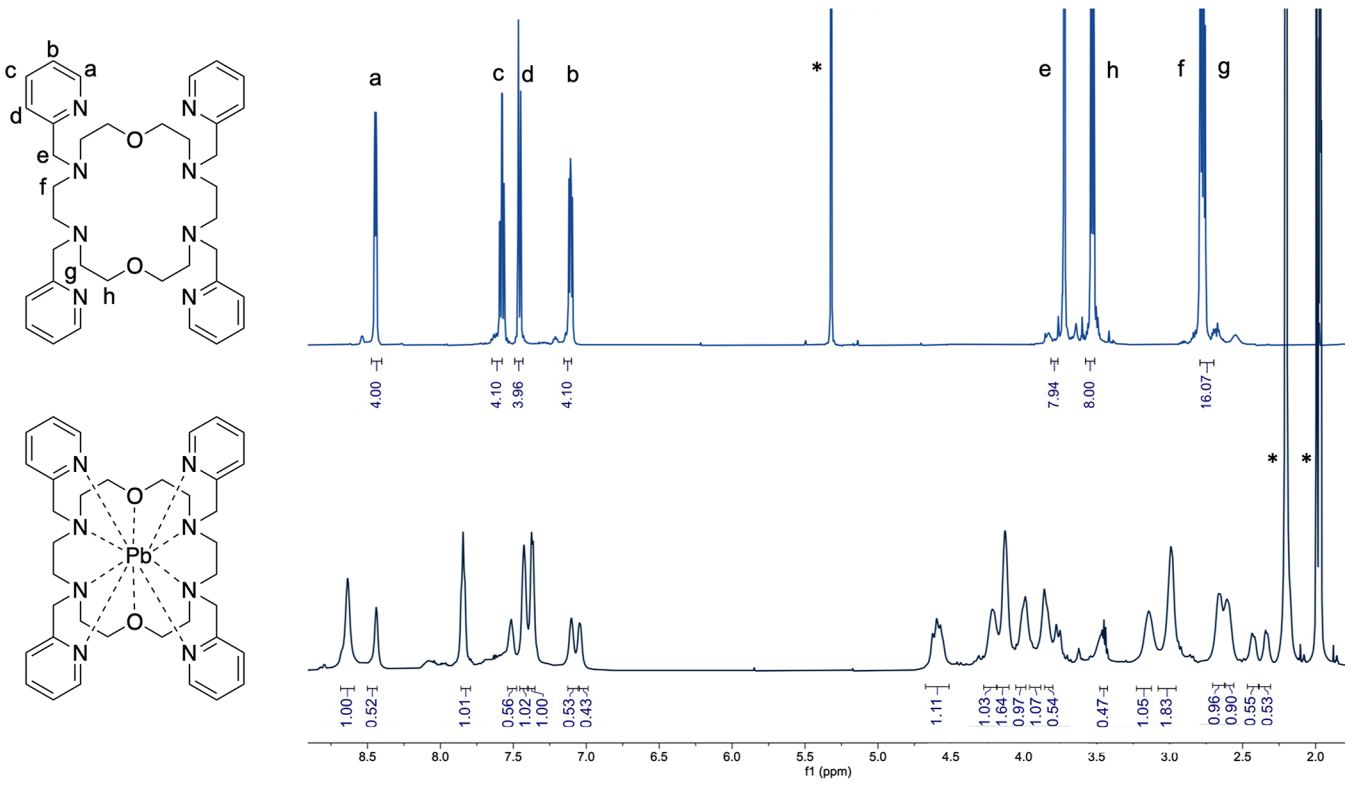

Figure 5. ^{1}H NMR spectra at 25 °C of Crown-4Py showing changes upon Pb^{2+}complexation. Top: Crown-4Py (500 MHz, CD_2Cl_2-d_2). Bottom: $[Pb(Crown\text{-}4Py)]^{2+}$ (600 MHz, CD_3CN-d_3). *Residual solvent peak.

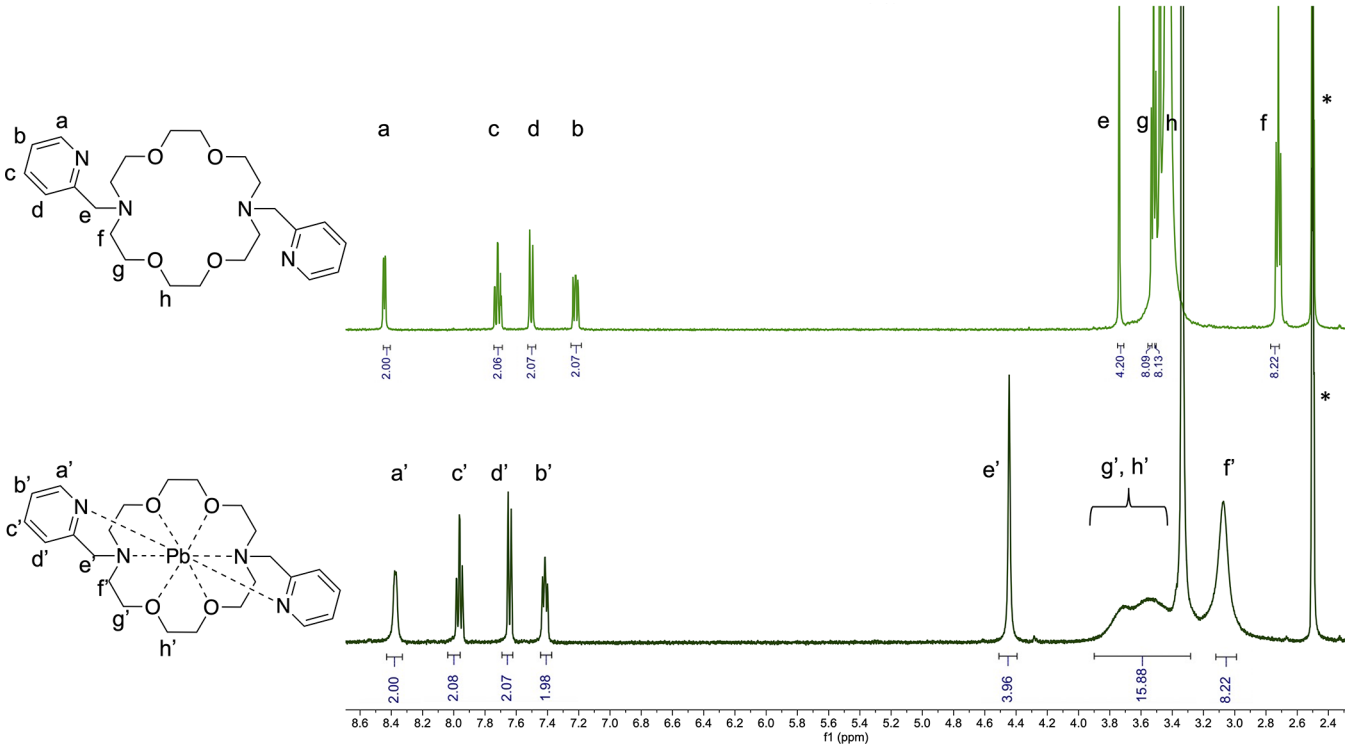

Figure 6. ^{1}H NMR spectra at 25 °C of NOON-2Py showing changes upon Pb^{2+}complexation. Top: NOON-2Py (400 MHz, DMSO-d_6). Bottom: $[Pb(NOON\text{-}2Py)]^{2+}$ (500 MHz, DMSO-d6). *Residual solvent peak.

large void in a coordination complex can be an issue for radiopharmaceuticals as it can allow for coordination by a competing, metal-seeking endogenous protein or biomolecule *in vivo*.[37] However, the thermodynamic favorability of complexation in the solution state cannot be determined from the crystal structure, and although mass spectrometry has been utilized and can provide information on the composition of the coordination complex, it cannot provide any information

https://doi.org/10.1021/acs.inorgchem.2c01114
Inorg. Chem. 2022, 61, 9638−9649

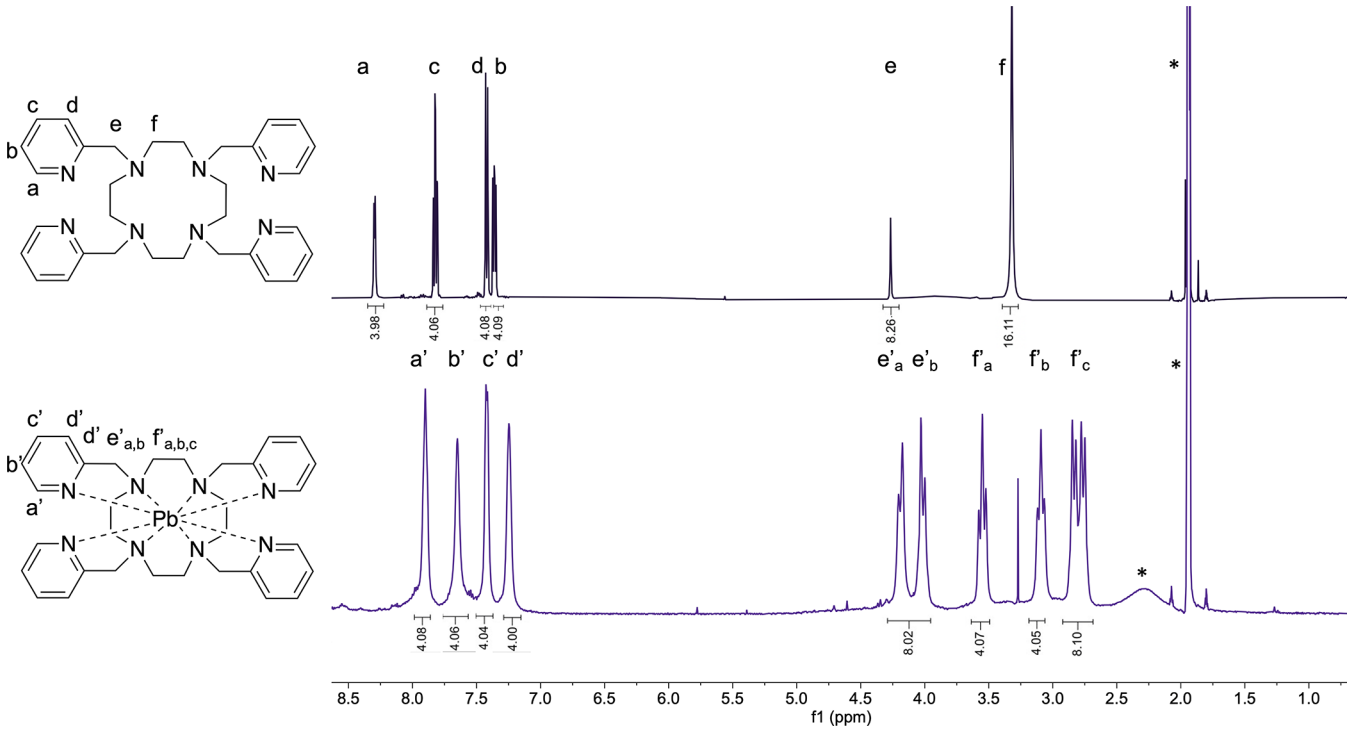

Figure 7. ^{1}H NMR spectra at 25 °C of Cyclen-4Py showing changes upon Pb^{2+}complexation. Top: Cyclen-4Py (400 MHz, CD_3CN-d_3). Bottom: $[Pb(Cyclen\text{-}4Py)]^{2+}$ (500 MHz, CD_3CN-d_3). *Residual solvent peak and water.

Table 4. Chelator Protonation Constants and Thermodynamic Stability Constants of Pb^{2+} Complexes[a]

	DOTA[38]	NOON-2Py[17]	Crown-4Py	Cyclen-4Py	DOTAM[40]
log K_1	12.09	7.44	7.91(4)	10.05(4)	7.70(1)
log K_2	9.76	6.26	7.33(4)	7.53(2)	6.21(1)
log K_3	4.559	1.38	4.64(1)	3.54(7)	
log K_4	4.09		4.00(6)	2.23(6)	
log K_{PbL}	25.3(1)[39]	11.67	13.29(5)	19.95(3)	>19
log K_{PbHL}			5.22(1)	2.06(9)	
log K_{PbH2L}			3.50(8)		
log K'_{Pb}[b]	15.64	11.33	12.45	16.93	
pPb[c]	20[39]	12.29	13.40	17.88	

[a][I = 0.1 M KCl for NOON-2Py, Crown-4Py, and Cyclen-4Py; I = 0.1 M $NaNO_3$ for DOTAM, 0.1 M Me_4NNO_3,[38] or 0.1 M NaCl[39] for DOTA] [b]Conditional stability constants (log K'_{Pb}) at pH 7.4, 25 °C, and I = 0.1 M. [c]pPb values calculated from $-\log [Pb]_{free}$ ($[Pb]_{tot} = 10^{-6}$ M, $[L]_{tot} = 10^{-5}$ M, pH 7.4, 25 °C, and I = 0.1 M).

on stability or how the complex acts in solution. Therefore, an investigation by solution-state NMR and potentiometry was necessary.

Literature precedence suggests that in solution, macrocyclic complexes, particularly polyether complexes, can exhibit dynamic and fluxional behavior that can make the analysis of NMR spectroscopic data difficult, limiting its utility.[31] This fluxional nature was apparent in the spectrum of the Pb^{2+} complexes of crown-4Py and NOON-2Py, as shown in Figures 5 and 6, respectively. In the ^{1}H NMR spectrum of $[Pb(Crown\text{-}4Py)]^{2+}$, the broadening of the peaks correlating to both the backbone and pyridine groups indicates that complexes form multiple isomers in solution, suggesting fluxional coordination, which can cause incompatibility *in vivo*. However, with $[Pb(NOON\text{-}2Py)]^{2+}$, this behavior is only evident for the hydrogen atoms belonging to the backbone (H_f, H_g, H_h), suggesting that the macrocycle undergoes dynamic changes at the NMR timescale, while the coordinating pyridine moieties do not. For the cyclen-4Py complex, one highly symmetric isomer is observed in solution. All methylene hydrogens (H_e and H_f), shown in Figure 7, are no longer equivalent and are diastereotopic as they exist in different chemical environments due to the formation of this complex. A single isomer in solution is advantageous as these complexes tend to be more stable *in vivo*, although this is not a reliable measure of absolute stability. A single isomer will lower the entropic penalty that the chelators face upon complexation as reorganization is not continually occurring. Although these NMR studies give insight into what is occurring in the solution state, the thermodynamic stability in solution can be quantitatively determined by potentiometry.

The protonation constants (log K_a) of the pyridyl chelators and the thermodynamic stability constants (log K_{ML}) of the Pb^{2+} complexes were determined by potentiometric titration in 0.1 M KCl, as shown in Table 4 and in Figures S20−23. However, thermodynamic stability constants alone are not adequate to predict and compare the stability of the complexes under physiological conditions, and so the more representative

https://doi.org/10.1021/acs.inorgchem.2c01114
Inorg. Chem. 2022, 61, 9638−9649

conditional stability constant (log K'_{Pb}) and pM values were determined at pH 7.4 and 25 °C. The pM values were calculated at a metal concentration of 1 μM and chelator concentration of 10 μM. The absence of accurately determined thermodynamic stability constants for Pb-DOTAM in the literature precluded calculation of conditional stability constants (log K'_{Pb}) and pM values for this metal−ligand complex, thus herein log K_{ML} for Pb-DOTAM are also discussed.

Of the pyridyl chelators tested, cyclen-4Py has the largest log K_{ML} and pM value of 19.95(3) and 17.88, respectively. Both the NMR spectrum, which showed one highly symmetric isomer in solution, and the solid-state structure, which showed Pb^{2+} was easily accessed by the pyridyl donor groups, can explain the high ^{203}Pb RCY with cyclen-4Py, suggesting that the smaller cyclen backbone is ideal when incorporating bulky donor groups into the design of a tailored lead(II) chelator. These constants and speciation diagrams can be of great use to predict the ideal pH for radiolabeling and the suitability of a chelator for a given metal; however, it is important to note that differences can arise at the tracer level used for radiopharmaceuticals, which may explain why DOTAM had a greater RCY than cyclen-4Py, but DOTA did not. At the tracer level, the chelator is in excess by orders of magnitude compared to the radiometal, whereas in these studies, the metal:chelator ratio is either 1:1 or 1:10, a ratio unlikely to be reached with radiolabeling.

Given that this structure−activity relationship study was meant to advance the use of ^{203}Pb/^{212}Pb radiopharmaceuticals, it would be of great interest to explore if this trend extends to bismuth (Bi^{3+}) as ^{212}Bi ($t_{1/2}$ = 60.55 min) is the α-emitting daughter of ^{212}Pb. Additionally, nonradioactive Bi^{3+} complexes of cyclen-4Py have been shown to possess anticancer activity *in vitro*;[41] Bi^{3+} complexation[20,22] and [^{213}Bi]Bi^{3+} radiolabeling studies[22] have been previously conducted with this chelator and results indicate that further investigation with this element is justified. Most of all, Bi^{3+}, like Pb^{2+}, has the potential to possess a stereochemically active lone pair. Additionally, future studies to observe if these findings can be extrapolated to intermediate Lewis bases with a smaller ionic radius, like Cu^{2+}, could provide insight on how to optimize chelator design in radiopharmaceuticals to improve metal selectivity and complex stability.

CONCLUSIONS

In summary, this study has demonstrated that when incorporating sterically hindered donor groups, pyridines in this study, the presence and size of the macrocyclic backbone have a significant effect on complex stability and feasibility for use in lead(II) radiopharmaceuticals. Through XRD, NMR spectroscopy, and potentiometric titration studies, it was found that Pb-complexation with smaller backbones (i.e., cyclen) causes the formation of facial complexes, which are more favorable allowing the metal to be more available for exocyclic coordination by the bulky donor groups, reducing conformational flexibility, and increasing the thermodynamic favorability of complexation compared to larger backbones with endocyclic coordination. With larger backbones (i.e., N_2O_4), reducing the number of bulky donor groups can improve accessibility to the metal, but the $6s^2$ lone pair belonging to lead, if stereochemically active, can cause a void in the coordination sphere, which can make the chelator incompatible with radiopharmaceutical applications. This work demonstrates the challenges associated with designing chelators for Pb-based radiopharmaceuticals. Moreover, cyclen-4Py holds the most promise of these pyridyl-containing chelators for elaboration into a radiopharmaceutical, as it exhibits high radio-lead incorporation yields at ambient temperatures and forms a kinetically inert [^{203}Pb]Pb-complex.

ASSOCIATED CONTENT

Supporting Information

The Supporting Information is available free of charge at https://pubs.acs.org/doi/10.1021/acs.inorgchem.2c01114.

Reaction schemes, ^{1}H/^{13}C/COSY/HSQC NMR spectra of several chelators and Pb^{2+} complexes, tabulated results of kinetic inertness studies, pH-potentiometric titration plots, solid-state structures for $[Pb(Cyclen)]^{2+}$, $[Pb(N_2O_4)]^{2+}$, and $[Pb(N_4O_2)]^{2+}$, and crystallographic information files (CIF) for the X-ray crystal structures along with relevant distance and bond angle data (PDF)

Accession Codes

CCDC 2160767−2160772 contain the supplementary crystallographic data for this paper. These data can be obtained free of charge via www.ccdc.cam.ac.uk/data_request/cif, or by emailing data_request@ccdc.cam.ac.uk, or by contacting The Cambridge Crystallographic Data Centre, 12 Union Road, Cambridge CB2 1EZ, UK; fax: +44 1223 336033.

AUTHOR INFORMATION

Corresponding Author

Caterina F. Ramogida − *Department of Chemistry, Simon Fraser University, Burnaby, British Columbia V5A 1S6, Canada; Life Sciences Division, TRIUMF, Vancouver, British Columbia V6T 2A3, Canada;* orcid.org/0000-0003-4815-2647; Email: cfr@sfu.ca

Authors

Brooke L. McNeil − *Department of Chemistry, Simon Fraser University, Burnaby, British Columbia V5A 1S6, Canada; Life Sciences Division, TRIUMF, Vancouver, British Columbia V6T 2A3, Canada*

Karthika J. Kadassery − *Department of Chemistry and Chemical Biology, Cornell University, Ithaca, New York 14853-1301, United States*

Anthony W. McDonagh − *Department of Chemistry, Simon Fraser University, Burnaby, British Columbia V5A 1S6, Canada*

Wen Zhou − *Department of Chemistry, Simon Fraser University, Burnaby, British Columbia V5A 1S6, Canada*

Paul Schaffer − *Department of Chemistry, Simon Fraser University, Burnaby, British Columbia V5A 1S6, Canada; Life Sciences Division, TRIUMF, Vancouver, British Columbia V6T 2A3, Canada; Department of Radiology, The University of British Columbia, Vancouver, British Columbia V5Z 1M9, Canada;* orcid.org/0000-0002-6392-8792

Justin J. Wilson − *Department of Chemistry and Chemical Biology, Cornell University, Ithaca, New York 14853-1301, United States;* orcid.org/0000-0002-4086-7982

Complete contact information is available at: https://pubs.acs.org/10.1021/acs.inorgchem.2c01114

Notes

The authors declare no competing financial interest.

https://doi.org/10.1021/acs.inorgchem.2c01114
Inorg. Chem. 2022, 61, 9638−9649

■ ACKNOWLEDGMENTS

Funding for this work was provided by the Natural Sciences and Engineering Research Council (NSERC) of Canada Discovery Grant (CFR, RGPIN-2019-07207; PS, RGPIN-2021-04093) and a Social Sciences and Humanities Research Council (SSHRC) of Canada New Frontiers in Research Fund Exploration Grant (CFR, NFRFE- 2018-00499). The US National Institutes of Health National Institute of Biomedical Imaging and Bioengineering supported this research in the lab of JJW under award numbers R21EB027282 and R01EB029259. TRIUMF receives funding via a contribution agreement with the Natural Research Council of Canada.

■ REFERENCES

(1) Okoye, N. C.; Baumeister, J. E.; Khosroshahi, F. N.; Hennkens, H. M.; Jurisson, S. S. Chelators and Metal Complex Stability for Radiopharmaceutical Applications. *Radiochim. Acta* **2019**, *107*, 1087−1120.

(2) Zukotynski, K.; Jadvar, H.; Capala, J.; Fahey, F. Targeted Radionuclide Therapy: Practical Applications and Future Prospects. *Biomarkers Cancer* **2016**, *8*, 35−38.

(3) Miller, C.; Rousseau, J.; Ramogida, C. F.; Celler, A.; Rahmim, A.; Uribe, C. F. Implications of Physics, Chemistry and Biology for Dosimetry Calculations Using Theranostic Pairs. In *Theranostics*; Ivyspring International Publisher, 2022; pp 232−259 DOI: 10.7150/THNO.62851.

(4) Ballinger, J. R. Theranostic Radiopharmaceuticals: Established Agents in Current Use. *Br. J. Radiol.* **2018**, *91*, No. 20170969.

(5) Rösch, F.; Herzog, H.; Qaim, S. M. The Beginning and Development of the Theranostic Approach in Nuclear Medicine, as Exemplified by the Radionuclide Pair 86 Y and 90 Y. *Pharmaceuticals* **2017**, *10*, No. 56.

(6) Delpassand, E. S.; Tworowska, I.; Esfandiari, R.; Torgue, J.; Hurt, J.; Shafie, A.; Núñez, R. Targeted Alpha-Emitter Therapy With ^{212}Pb-DOTAMTATE for the Treatment of Metastatic SSTR-Expressing Neuroendocrine Tumors: First-in-Human, Dose-Escalation Clinical Trial. *J. Nucl. Med.* **2022**, No. 263230.

(7) Ray Banerjee, S.; Pullambhatla, M.; Foss, C. A.; Falk, A.; Byun, Y.; Nimmagadda, S.; Mease, R. C.; Pomper, M. G. Effect of Chelators on the Pharmacokinetics of 99mTc-Labeled Imaging Agents for the Prostate-Specific Membrane Antigen (PSMA). *J. Med. Chem.* **2013**, *56*, 6108.

(8) Price, E. W.; Orvig, C. Matching Chelators to Radiometals for Radiopharmaceuticals. *Chem. Soc. Rev.* **2014**, *43*, 260−290.

(9) Hancock, R. D.; Martell, A. E. Ligand Design for Selective Complexation of Metal Ions in Aqueous Solution. *Chem. Rev* **1989**, *89*, 1875−1914.

(10) Pearson, R. G. Hard and Soft Acids and Bases. *J. Am. Chem. Soc.* **1963**, *85*, 3533−3539.

(11) Pearson, R. G. Hard and Soft Acids and Bases, HSAB, Part I: Fundamental Principles. *J. Chem. Educ.* **1968**, *45*, 581−587.

(12) Pearson, R. G. Hard and Soft Acids and Bases, HSAB, Part II: Underlying Theories. *J. Chem. Educ.* **1968**, *45*, 643−648.

(13) Chappell, L. L.; Dadachova, E.; Milenic, D. E.; Garmestani, K.; Wu, C.; Brechbiel, M. W. Synthesis, Characterization, and Evaluation of a Novel Bifunctional Chelating Agent for the Lead Isotopes ^{203}Pb and ^{212}Pb. *Nucl. Med. Biol.* **2000**, *27*, 93−100.

(14) Holbein, B. E.; Ang, M. T. C.; Allan, D. S.; Chen, W.; Lehmann, C. Iron-Withdrawing Anti-Infectives for New Host-Directed Therapies Based on Iron Dependence, the Achilles' Heel of Antibiotic-Resistant Microbes. *Environ. Chem. Lett.* **2021**, *19*, 2789−2808.

(15) Gode, F.; Pehlivan, E. A Comparative Study of Two Chelating Ion-Exchange Resins for the Removal of Chromium(III) from Aqueous Solution. *J. Hazard. Mater.* **2003**, *100*, 231−243.

(16) Ferreirós-Martínez, R.; Esteban-Gómez, D.; Tóth, E.; De Blas, A.; Platas-Iglesias, C.; Rodríguez-Blas, T. Macrocyclic Receptor Showing Extremely High Sr(II)/Ca(II) and Pb(II)/ Ca(II) Selectivities with Potential Application in Chelation Treatment of Metal Intoxication. *Inorg. Chem.* **2011**, *50*, 3772−3784.

(17) Damu, K. V.; Shaikjee, M. S.; Michael, J. P.; Howard, A. S.; Hancock, R. D. Control of Metal Ion Selectivity in Ligands Containing Neutral Oxygen and Pyridyl Groups. *Inorg. Chem.* **1986**, *25*, 3879−3883.

(18) Tétard, D.; Rabion, A.; Verlhac, J. B.; Guilhem, J. Alkane Hydroxylation by a Manganese Analogue of the Iron Core from Methane Monooxygenase. *J. Chem. Soc., Chem. Commun.* **1995**, 531−532.

(19) Bu, X.-H.; Cao, X.-C.; Zhang, W.-Q.; Zhang, R.-H.; Clifford, T. A New Tetraazamacrocycle Functionalized with Pendant Pyridyl Groups: Synthesis and Crystal Structure of a Copper (II) Complex Of. *Transition Metal Chemistry* **1997**, *22*, 513−515.

(20) Morfin, J. F.; Tripier, R.; Baccon, M.; le Handel, H. Bismuth(III) Complexes with Tetra-Pyridylmethyl-Cyclen. *Inorg. Chim. Acta* **2009**, *362*, 1781−1786.

(21) Wilson, J. J.; Birnbaum, E. R.; Batista, E. R.; Martin, R. L.; John, K. D. Synthesis and Characterization of Nitrogen-Rich Macrocyclic Ligands and an Investigation of Their Coordination Chemistry with Lanthanum(III). *Inorg. Chem.* **2015**, *54*, 97−109.

(22) Wilson, J. J.; Ferrier, M.; Radchenko, V.; Maassen, J. R.; Engle, J. W.; Batista, E. R.; Martin, R. L.; Nortier, F. M.; Fassbender, M. E.; John, K. D.; Birnbaum, E. R. Evaluation of Nitrogen-Rich Macrocyclic Ligands for the Chelation of Therapeutic Bismuth Radioisotopes. *Nucl. Med. Biol.* **2015**, *42*, 428−438.

(23) Yang, H.; Zhang, C.; Yuan, Z.; Rodriguez-Rodriguez, C.; Robertson, A.; Radchenko, V.; Perron, R.; Gendron, D.; Causey, P.; Gao, F.; Bénard, F.; Schaffer, P. Synthesis and Evaluation of a Macrocyclic Actinium-225 Chelator, Quality Control and In Vivo Evaluation of ^{225}Ac-Crown-AMSH Peptide. *Chem. − Eur. J.* **2020**, *26*, 11435−11440.

(24) McNeil, B. L.; Robertson, A. K. H.; Fu, W.; Yang, H.; Hoehr, C.; Ramogida, C. F.; Schaffer, P. Production, Purification, and Radiolabeling of the ^{203}Pb/^{212}Pb Theranostic Pair. *EJNMMI Radiopharm. Chem.* **2021**, *6*, No. 6.

(25) Altomare, A.; Cascarano, G.; Giacovazzo, C.; Guagliardi, A. Completion and Refinement of Crystal Structures with SIR92. *J. Appl. Crystallogr.* **1993**, *26*, 343−350.

(26) Altomare, A.; Burla, M. C.; Camalli, M.; Cascarano, G. L.; Giacovazzo, C.; Guagliardi, A.; Moliterni, A. G. G.; Polidori, G.; Spagna, R. SIR97: A New Tool for Crystal Structure Determination and Refinement. *J. Appl. Crystallogr.* **1999**, *32*, 115−119.

(27) Farrugia, L. J. WinGX Suite for Small-Molecule Single-Crystal Crystallography. *J. Appl. Crystallogr.* **1999**, *32*, 837−838.

(28) Sweeton, F. H.; Mesmer, R. E.; Baes, C. F. Acidity Measurements at Elevated Temperatures. VII. Dissociation of Water. *J. Solution Chem.* **1974**, *3*, 191−214.

(29) Gans, P.; O'Sullivan, B. GLEE, a New Computer Program for Glass Electrode Calibration. *Talanta* **2000**, *51*, 33−37.

(30) Gans, P.; Sabatini, A.; Vacca, A. Investigation of Equilibria in Solution. Determination of Equilibrium Constants with the HYPERQUAD Suite of Programs. *Talanta* **1996**, *43*, 1739−1753.

(31) Swidan, A.; Macdonald, C. L. B. Polyether Complexes of Groups 13 and 14. *Chem. Soc. Rev.* **2016**, *45*, 3883−3915.

(32) Steed, J. W. First- and Second-Sphere Coordination Chemistry of Alkali Metal Crown Ether Complexes. *Coord. Chem. Rev.* **2001**, *215*, 171−221.

(33) Shannon, R. D. Revised Effective Ionic Radii and Systematic Studies of Interatomie Distances in Halides and Chaleogenides. *Acta Crystallogr., Sect. A: Found. Adv.* **1976**, *A32*, 751−767.

(34) Bird, C. W.; Cheeseman, G. W. H. Structure of Five-Membered Rings with One Heteroatom. *Compr. Heterocycl. Chem.* **1984**, *4*−*7*, 1−38.

(35) Hancock, R. D. Chelate Ring Size and Metal Ion Selection: The Basis of Selectivity for Metal Ions in Open-Chain Ligands and Macrocycles. *J. Chem. Educ.* **1992**, *69*, 615−621.

https://doi.org/10.1021/acs.inorgchem.2c01114
Inorg. Chem. 2022, 61, 9638−9649

(36) Shimoni-Livny, L.; Glusker, J. P.; Bock, C. W. Lone Pair Functionality in Divalent Lead Compounds. *Inorg. Chem.* **1998**, *37*, 1853−1867.
(37) Ingham, A.; Kostelnik, T. I.; McNeil, B. L.; Patrick, B. O.; Choudhary, N.; Jaraquemada-Peláez, M. de G.; Orvig, C. Getting a Lead on Pb^{2+}-Amide Chelators for $^{203/212}Pb$ Radiopharmaceuticals. *Dalton Trans.* **2021**, *50*, 11579−11595.
(38) Chaves, S.; Delgado, R.; da Silva, J. J. R. F. The Stability of the Metal Complexes of Cyclic Tetra-Aza Tetra-Acetic Acids. *Talanta* **1992**, *39*, 249−254.
(39) Tosato, M.; Lazzari, L.; Marco, V. di. Revisiting Lead(II)-1,4,7,10-Tetraazacyclododecane-1,4,7,10-Tetraacetic Acid Coordination Chemistry in Aqueous Solutions: Evidence of an Underestimated Thermodynamic Stability. *ACS Omega* **2022**, *7*, 15596−15602.
(40) Maumela, H.; Hancock, R. D.; Carlton, L.; Reibenspies, J. H.; Wainwright, K. P. The Amide Oxygen as a Donor Group. Metal Ion Complexing Properties of Tetra-A-Acetamide Substituted Cyclen: A Crystallographic, NMR, Molecular Mechanics, and Thermodynamic Study. *J. Am. Chem. Soc.* **1995**, *117*, 6698−6707.
(41) Wang, X.; Zhang, X.; Lin, J.; Chen, J.; Xu, Q.; Guo, Z. DNA-Binding Property and Antitumor Activity of Bismuth(III) Complex with 1,4,7,10-Tetrakis(2-Pyridylmethyl)-1,4,7,10-Tetraazacyclododecane. *Dalton Trans.* **2003**, 2379−2380.

Recommended by ACS

Chelating the Alpha Therapy Radionuclides 225Ac3+ and 213Bi3+ with 18-Membered Macrocyclic Ligands Macrodipa and Py-Macrodipa

Aohan Hu, Justin J. Wilson, *et al.*

DECEMBER 29, 2021
INORGANIC CHEMISTRY

READ

Stable Chelation of the Uranyl Ion by Acyclic Hexadentate Ligands: Potential Applications for 230U Targeted α-Therapy

Joshua J. Woods, Justin J. Wilson, *et al.*

FEBRUARY 09, 2022
INORGANIC CHEMISTRY

READ

232Th-Spallation-Produced 225Ac with Reduced 227Ac Content

Andrew K. H. Robertson, Paul Schaffer, *et al.*

JULY 17, 2020
INORGANIC CHEMISTRY

READ

H2BZmacropa-NCS: A Bifunctional Chelator for Actinium-225 Targeted Alpha Therapy

Karthika J. Kadassery, Justin J. Wilson, *et al.*

JUNE 07, 2022
BIOCONJUGATE CHEMISTRY

READ

Get More Suggestions >

https://doi.org/10.1021/acs.inorgchem.2c01114
Inorg. Chem. 2022, 61, 9638−9649